Fang, Yu Huang; Liang, Chen; Liljeström, Ville; Lv, Zhong Peng; Ikkala, Olli; Zhang, Hang

Toughening Hydrogels with Fibrillar Connected Double Networks

Published in:
Advanced Materials

DOI:
10.1002/adma.202402282

Published: 04/07/2024

Document Version
Publisher's PDF, also known as Version of record

ADVANCED MATERIALS
www.advmat.de

Toughening Hydrogels with Fibrillar Connected Double Networks

*Yu-Huang Fang, Chen Liang, Ville Liljeström, Zhong-Peng Lv, Olli Ikkala, and Hang Zhang**

Biological tissues, such as tendons or cartilage, possess high strength and toughness with very low plastic deformations. In contrast, current strategies to prepare tough hydrogels commonly utilize energy dissipation mechanisms based on physical bonds that lead to irreversible large plastic deformations, thus limiting their load-bearing applications. This article reports a strategy to toughen hydrogels using fibrillar connected double networks (fc-DN), which consist of two distinct but chemically interconnected polymer networks, that is, a polyacrylamide network and an acrylated agarose fibril network. The fc-DN design allows efficient stress transfer between the two networks and high fibril alignment during deformation, both contributing to high strength and toughness, while the chemical crosslinking ensures low plastic deformations after undergoing high strains. The mechanical properties of the fc-DN network can be readily tuned to reach an ultimate tensile strength of 8 MPa and a toughness of above 55 MJ m^{-3}, which is 3 and 3.5 times more than that of fibrillar double network hydrogels without chemical connections, respectively. The application potential of the fc-DN hydrogel is demonstrated as load-bearing damping material for a jointed robotic lander. The fc-DN design provides a new toughening mechanism for hydrogels that can be used for soft robotics or bioelectronic applications.

1. Introduction

Human bodies consist of many load-bearing soft tissues, including muscle, cartilage, tendon, and ligament, which possess excellent mechanical properties.[1] For instance, tendons are robust connective tissues that link muscles to bones, as well as to other tissues, which can withstand a high tensile stress exceeding 50 MPa.[2] One notable feature of these tough tissues is their low plastic deformation under load, which makes them perfect load-bearing components in biological systems.[3–5] In contrast to natural load-bearing tissues, conventional hydrogels are usually soft, weak, and brittle due to the low density of polymer chains and heterogeneous polymer networks, which hinder their use in applications requiring high load tolerance.[6,7] To date, considerable efforts have been devoted to strengthening and toughening hydrogels by building effective energy dissipation mechanisms into polymer networks such as by introducing hydrophobic interactions,[8,9] electrostatic interactions,[10–12] hydrogen bonds,[13–15] coordination complexes,[16–18] host–guest interactions,[19,20] helical associations,[21–23] releasable extra chains,[24] hard domains,[25] and crystalline domains.[26,27] For instance, He et al. employed an ice-templated freeze-casting strategy to impart strong aggregation of hydrogen bonds and crystalline domains to a polyvinyl alcohol hydrogel, resulting in substantial reinforcement and toughening.[27] These methods primarily focus on molecular engineering, while other systems adopt structural engineering approaches such as using multiple networks,[28] stretching-induced alignment,[29,30] 2D hierarchical structures,[31,32] and dense entanglements of polymer chains.[33–35] Despite the remarkable progress, the toughening mechanisms in hydrogels typically involve plastic deformations, such as by introducing crystallizations or hard domains,[25,27] that are often characterized by the presence of yield behavior.

Interpenetrating polymer network (IPN) hydrogels consist of two or more interpenetrated polymer networks, which are individually crosslinked, that is, they are not chemically connected.[36,37] Gong et al. first developed a new class of IPN hydrogel, known as the double-network (DN) hydrogels, which exhibited significantly enhanced strength and toughness compared to single-network hydrogels.[28] The essential feature of DN hydrogels is the presence of two distinct types of polymer networks with asymmetric structures, which differ from conventional IPN.[38–41] The existence of a brittle internal network acts as a sacrificial structure, endowing remarkable toughness to the

Y.-H. Fang, C. Liang, Z.-P. Lv, O. Ikkala, H. Zhang
Department of Applied Physics
Aalto University
P.O. Box 15100, Espoo 02150, Finland
E-mail: hang.zhang@aalto.fi
V. Liljeström
Nanomicroscopy Center, OtaNano
Aalto University
P.O. Box 15100, Espoo 02150, Finland

The ORCID identification number(s) for the author(s) of this article can be found under https://doi.org/10.1002/adma.202402282

DOI: 10.1002/adma.202402282

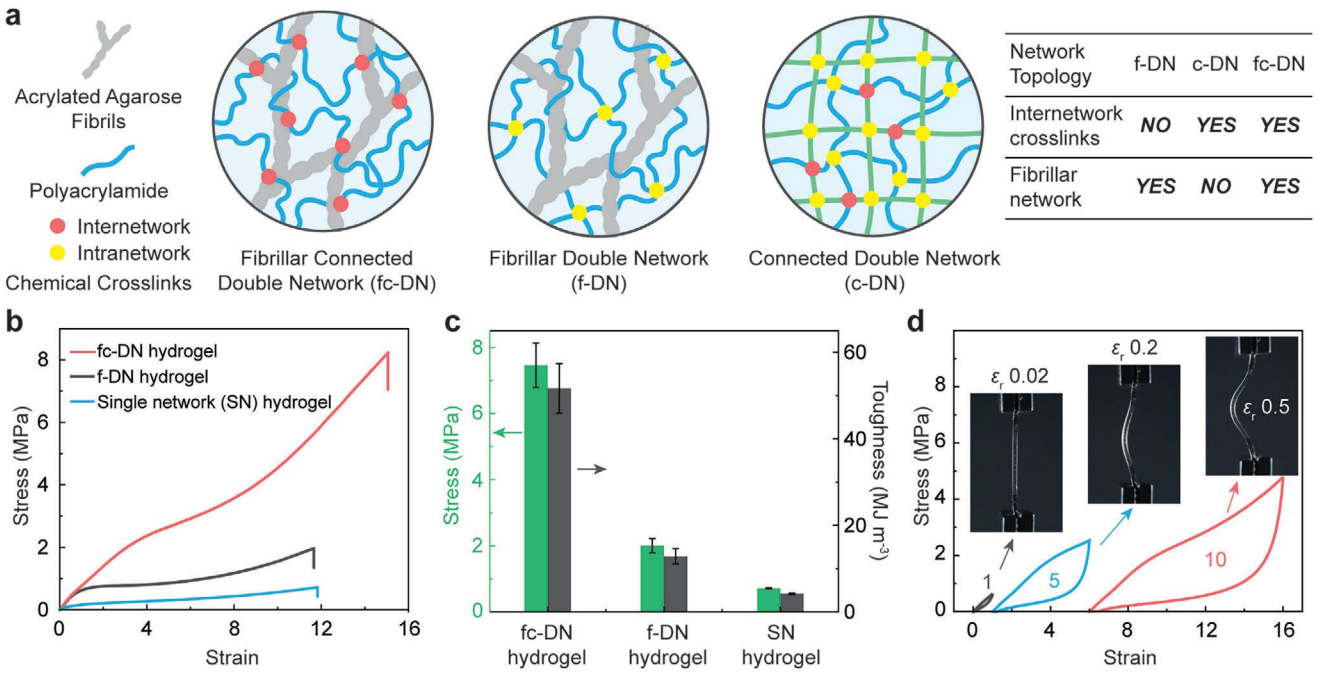

Figure 1. Tough AcAG/PAAm fc-DN hydrogel. a) Schematic illustrations for three different DN topologies in hydrogels. b) Tensile stress–strain curves of AcAG/PAAm fc-DN hydrogel, AG/PAAm f-DN hydrogel, and PAAm SN hydrogel. DA = 30%, $C_{AcAG} = C_{AG} = 3$ wt%, $C_{AAm} = 50$ wt%, $C_{CL} = 0.02$ mol%. c) A comparison of fracture strength and toughness of the three types of hydrogels. d) Cyclic tensile tests of fc-DN hydrogels. Insets are the optical images of the fc-DN hydrogel after one cycle of stretching and full recovery of strain.

hydrogel. This principle enables the hydrogel to surpass the performance of its individual networks and even reach mechanical properties comparable to certain soft load-bearing tissues. For instance, Wiley et al. reported a 3D-printed DN hydrogel with a compression strength and elastic modulus greater than those of cartilage.[42] Recently, a self-growing trainable hydrogel based on the DN approach has been demonstrated.[43] Through repeated mechanical stresses that break the brittle network and a continuous supply of monomers, the hydrogel progressively strengthens due to the polymerization of the monomers onto the broken sites. On the other hand, other types of IPN hydrogels with enhanced mechanical properties have been developed. For example, Pan et al. developed a novel IPN hydrogel that exhibits high compressive strength and toughness by using a copolymer as the primary network.[44] The improvement of mechanical properties is mainly attributed to the higher strength of the primary network and stronger interactions between the two networks.[44] IPN hydrogels based on acrylamide-modified agar, oxidized alginate, and polyacrylamide (PAAm) have been synthesized with high stretchability and ionic conductivity.[45] Despite the great progress in designing tough IPN and DN hydrogels, the weak interactions between the two networks via hydrogen bonds, polymer entanglements, etc., is a limiting factor for the stress transfer from one network to another and thus the toughening behavior.

Here, we report a new design strategy to construct fibrillar connected double network (fc-DN) hydrogels with significantly improved toughness compared to conventional IPN and DN hydrogels, while maintaining low plastic deformations. The fc-DN hydrogel comprises of a PAAm network chemically crosslinked by an acrylated agarose (AcAG) fibril network as the macrocrosslinker. In this way, the fc-DN is essentially an interconnected interpenetrating network.[37] The main distinction between fc-DN and conventional DN lies in the simultaneous presence of a fibrillar first network, as well as the covalent crosslinks between the two networks in the fc-DN.[37,46] In previous reports, either the fibrillar first network[47] or chemical crosslinks between the two networks[23] are missing. The fc-DN strategy allows enhanced interfacial strength between the relatively soft and elastic PAAm network and the more rigid but brittle agarose fibrillar network, which undergoes a high degree of fibril alignment during large deformations. This leads to significantly enhanced strength and toughness compared to conventional DN hydrogels, yet still maintaining low plastic deformations after undergoing high strains. The mechanical properties of the fc-DN system can be readily tuned by the chemical composition and the density of crosslinks, providing a versatile toolbox for engineering the mechanical properties and especially the toughness of hydrogels.

2. Results and Discussion

2.1. Preparation of the fc-DN Hydrogel

The network design of fc-DN is shown in **Figures** 1a and S1b, Supporting Information, which is distinct from conventional fibrillar DN (f-DN)[23,45] or connected DN (c-DN).[47] The fc-DN most notably consists of a fibrillar first network and an elastic second polymeric network, which are chemically linked together via covalent bonds. In contrast, f-DN (e.g., Agar/PAAm hydrogel)[23] consists of a fibrillar first network and an elastic second network that is chemically independent of each other.

Besides, c-DN (e.g., poly(2-acrylamido-2- methylpropanesulfonic acid) (PAMPS)/PAAm DN)[47] contains two polymer networks that are chemically connected via covalent bonds, which, however, lacks a fibrillar network. To control chemical crosslinking between the two networks, we have modified natural agarose by partially replacing the hydroxyl groups on the agarose polymer chains with acrylate groups as shown in Figure S1a, Supporting Information.[46,48] The degree of acrylation (DA) is defined as the nominal molar ratio of acryloyl chloride to hydroxymethyl groups during the chemical modification process, as illustrated in Figure S2, Supporting Information. For instance, DA 30% means that 30 mol% of acryloyl chloride relative to the available hydroxymethyl groups was added during modification. The real degrees of substitution of the final product were determined by ^{1}H-NMR and shown in Figure S2 and Table S1, Supporting Information, which revealed degrees of substitution of 1.4% and 4.2% for DA 30% and 60%, respectively. For consistency, the DA is used throughout this manuscript, as the degree of substitution cannot be reliably determined via ^{1}H-NMR for very low feed ratios such as DA of 10%. The synthesis of the AcAG/PAAm fc-DN hydrogel is schematically shown in Figure S1a, Supporting Information, following a straightforward one-pot approach.[46] All reactants, that is, AcAG, AAm monomers, and photoinitiator, were first dissolved in water at 90 °C, i.e., above the melting point of AcAG, resulting in a transparent homogeneous solution. The hot solution was then transferred to a mold with the desired final shape (see Experimental Section for details). As the solution gradually cooled down to room temperature, the agarose formed the first physical network consisting of nanoscopic fibrils. SEM characterization of the agarose fibrils revealed an average diameter of 25 ± 5 nm (Figure S3, Supporting Information), similar to previous reports.[49] The acrylation did not seem to affect the microscopic structures of the agarose fibrils. Upon UV-initiation, the PAAm network was formed within the agarose network, where the acrylate groups on the AcAG serve as the chemical crosslinks between the two networks, leading to the fc-DN hydrogel. Chemical crosslinks within the AcAG network may also exist, as demonstrated by the increased mechanical properties in AcAG SN gel treated with UV and photoinitiator compared to pristine AcAG SN hydrogel (Figure S4, Supporting Information). However, such chemical crosslinks within the AcAG network do not seem to contribute to the mechanical reinforcement in the fc-DN hydrogel (Figure S5, Supporting Information), and they are thus not illustrated in Figure 1a. For the preparation of the AG/PAAm f-DN hydrogel, the same protocol was employed, except for using pristine agarose instead of AcAG and adding *N,N′*-methylenebis(acrylamide) (BIS) as the crosslinker.

Figure 1b,c demonstrates the significantly improved mechanical properties of AcAG/PAAm fc-DN hydrogel compared to AG/PAAm f-DN hydrogels and PAAm SN hydrogels. Here the fc-DN hydrogel contains 50 wt% PAAm and 3 wt% AcAG with a DA of 30%. It should be noted that these three different hydrogel topologies contained the same number of chemical crosslinking points, which means that the molar concentration of the crosslinker BIS in the AG/PAAm f-DN hydrogel and the PAAm SN hydrogel are the same as the molar concentration of acrylate groups in the AcAG/PAAm fc-DN hydrogel. For all hydrogels shown in Figure 1b, the crosslink-to-AAm monomer molar ratio C_{CL} is 0.02 mol%. For a detailed calculation of chemical crosslinking points, see the Supporting Information text. The fc-DN and f-DN should contain the same number of physical crosslinks since they consist of the same concentration of agarose and PAAm. The SN hydrogel contains less physical crosslinks than the fc-DN and f-DN due to the absence of the agarose network. In this work, the nominal stress at a constant tensile strain rate of 5 min^{-1} is reported, which is calculated as the force divided by the cross-sectional area of the pristine undeformed hydrogel. The AcAG/PAAm fc-DN hydrogels display a distinct strain-stiffening property at a strain above 10, reaching a maximum tensile stress of 8 MPa, which is 4 times and 11 times higher than that of AG/PAAm f-DN hydrogels (2 MPa) and PAAm SN hydrogels (0.7 MPa), respectively (Figure 1c). The fracture strain is ≈16 for fc-DN hydrogels and ≈12 for f-DN hydrogels and PAAm SN hydrogels. With higher fracture strain and strength, the toughness of AcAG/PAAm fc-DN hydrogels reaches 55 MJ m^{-3}, calculated from the area below the stress–strain curve, which far exceeds that of either AG/PAAm f-DN hydrogels (12 MJ m^{-3}) or PAAm SN hydrogels (4 MJ m^{-3}). Compared to previously reported PAMPS/PAAm c-DN hydrogels lacking a fibrillar network, the toughness is also significantly enhanced by 4 times in the fc-DN hydrogel.[50]

When pre-existing cracks are introduced, AcAG/PAAm fc-DN hydrogels exhibit a fracture toughness of 4.7 kJ m^{-2}, which is 2.35 times higher than the 2 kJ m^{-2} of AG/PAAm f-DN hydrogels (Figure S6, Supporting Information). The compressive mechanical property of AcAG/PAAm fc-DN hydrogels was also compared with that of AG/PAAm f-DN hydrogels and PAAm SN hydrogels. As shown in Figure S7, Supporting Information, when compressed to a strain of 0.9, AcAG/PAAm fc-DN hydrogels achieve a maximum compressive strength of 50 MPa without the sample failing. In contrast, the compressive strength is only 28 MPa for AG/PAAm f-DN hydrogels and 14 MPa for PAAm SN hydrogels. It is notable that AcAG/PAAm fc-DN hydrogels exhibit low residual strain ϵ_r as defined in Equation (1)

$$\epsilon_r = \frac{L_f}{L_0} - 1 \tag{1}$$

where L_f is the final zero-stress length of the sample after one loading–unloading cycle, and L_0 is the original length of the pristine sample. As shown in Figure 1d, the residual strains range between 0.02 and 0.5 in the strain range between 1 and 10. The hysteresis behaviors during cyclic tensile tests and toughening mechanism will be further discussed in the later section.

2.2. Tuning the Mechanical Properties in fc-DN Hydrogel

The mechanical properties of the fc-DN hydrogel can be readily tuned by varying the compositions such as the crosslinking density and concentrations of AAm and AcAG. We first demonstrate the effect of crosslinking density for AcAG/PAAm fc-DN hydrogels by varying the DA at a fixed monomer content of 50 wt% and AcAG content of 3 wt%. As shown in **Figure 2a** and Figure 2d, when varying DA from 10% to 30%, the strength and toughness of the fc-DN hydrogel increase as the DA increases, a common observation in polymeric systems at low crosslinking degrees.[51] At a DA of 30%, the fc-DN hydrogels exhibit the highest tensile

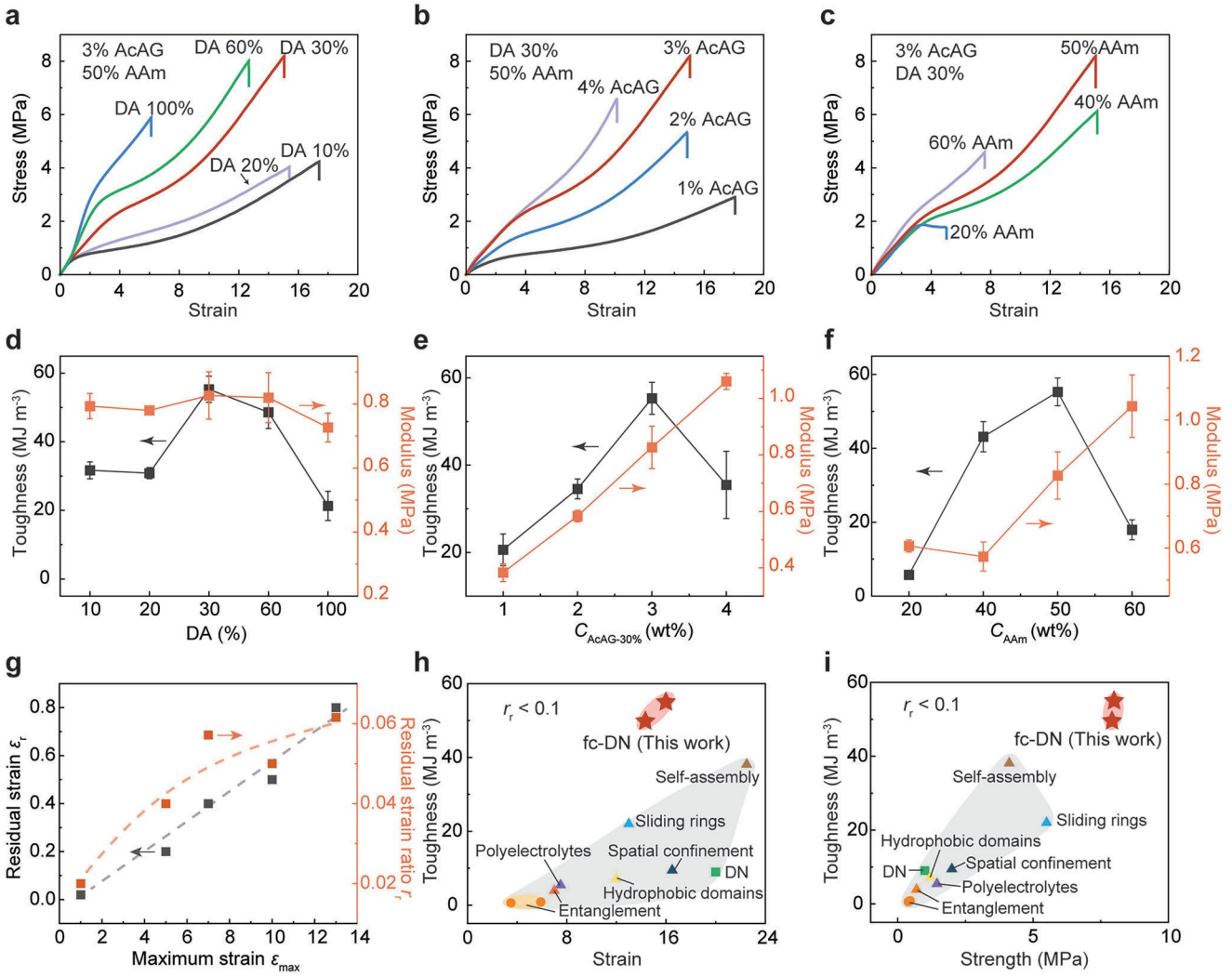

Figure 2. Tuning the mechanical properties of the AcAG/PAAm fc-DN hydrogels. a) Tensile stress–strain curves of hydrogels with varying DA. The hydrogels contained 50 wt% PAAm and 3 wt% AcAG. b) Tensile stress–strain curves of hydrogels with varying AcAG content. The hydrogels contained 50 wt% PAAm and AcAG with a DA of 30%. c) Tensile stress–strain curves of hydrogels with various AAm content. The hydrogels contained 3 wt% AcAG with a DA of 30%. d) Toughness and modulus as a function of DA respectively. e) Toughness and modulus as a function of AcAG content, respectively. f) Toughness and modulus as a function of AAm content, respectively. Error bars show standard deviations from three independent samples. g) Residual strain ϵ_r and residual strain ratio r_r of the AcAG/PAAm hydrogel as a function of maximum strain ϵ_{max}. DA = 30%, C_{AcAG} = 3 wt%, C_{AAm} = 50 wt%. h,i) Ashby diagrams of toughness versus fracture strain (h) and toughness versus ultimate tensile strength (i) of AcAG/PAAm fc-DN hydrogels and other reported tough hydrogels with low residual strain ratios ($\epsilon_{max} > 1$, $r_r < 0.1$, fracture strain < 25). The references are summarized in Table S2, Supporting Information.

strength (8 MPa) and the highest toughness (55 MJ m^{-3}). When the DA is above 60%, however, the strength, toughness, and fracture strain of the fc-DN hydrogels decrease as the DA increases. This is attributed to the dense crosslinking at high DA, which reduces the length of the polymer segments between each two crosslinking points that are often associated with stiffer and more brittle networks.[52,53] Further increasing the DA to 200% led to alternation of the gelation behavior of the AcAG, which could not form a gel when cooled to room temperature at a concentration of 3 wt% even after an extended period. Similar observations on modified agarose have been reported in the literature.[48] The fc-DN prepared with AcAG (DA 200%) shows low modulus and high brittleness in the tensile test (Figure S8a, Supporting Information), but with similar hysteresis behavior compared to other fc-DN hydrogels during cyclic tensile tests as shown in Figure S8b, Supporting Information. This indicates the presence of agarose fibrils at DA 200% that underwent permanent damage during stretching, though such highly modified agarose could not form a gel due to lack of a percolating network. The dispersed fibrillar structures of AcAG at DA 200% contributed to the higher mechanical strength in the fc-DN hydrogel compared to PAAm SN gel or fc-DN gel prepared at a temperature above the melting point of AcAG (i.e., without agarose fibrils, Figure S9, Supporting Information).

Figure 2b,e demonstrates the effect of AcAG content for AcAG/PAAm fc-DN hydrogels with AcAG content varying from

1 to 4 wt%. The modulus of the fc-DN hydrogels are almost monotonic functions of AcAG content. As the AcAG content increases from 1 to 4 wt%, the fracture strain decreases from 17 to 10, while the modulus increases from 0.4 MPa to over 1 MPa. On the other hand, the strength and toughness increase with increasing AcAG content below 3 wt%. The effect of AcAG content is twofold. First, AcAG provides a rigid first network in the fc-DN. With increasing AcAG content, the strength and stiffness of the first network increase, which results in rising strength and modulus of fc-DN hydrogels. Second, the AcAG provides crosslink points in the fc-DN hydrogel due to the presence of acrylate groups. It is well known that a critical value of crosslink density exists in the hydrogel, above which the hydrogel strength decreases with increasing crosslink density.[51] The decreasing hydrogel strength for AcAG above 3 wt% can be explained by the decrease in the length of PAAm segments between crosslinks, which results in restricted chain orientation and high stress due to pre-stretch.[53,54]

The effect of AAm content for AcAG/PAAm fc-DN hydrogels with a fixed DA of 30%, and fixed AcAG content of 3 wt% is shown in Figure 2c,f. When AAm content is below 50 wt%, the strength and toughness increase as AAm content increases. However, as AAm content increases to 60 wt%, the strength and toughness decrease dramatically. This is due to the insufficient gelation of AcAG at such a high monomer concentration, as evidenced by the weak agarose gel (Figure S10, Supporting Information). The underlying reason is that the high content of monomer interferes with the intermolecular interactions in agarose, hindering the formation of a strong fibrillar network. Similar to strength, the fracture strain increases from 5 to 15 as the AAm content increases from 20 to 50 wt%. However, when the AAm content reaches 60 wt%, the fracture strain experiences a significant decrease from 15 to 8. In comparison, the modulus increases from 0.6 to 1 MPa with increasing AAm content from 20 to 60 wt%.

To better describe and compare the residual (i.e., plastic) deformation of the fc-DN hydrogels under load with other reported tough hydrogels, we define residual strain ratio r_r in Equation (2)

$$r_r = \frac{\epsilon_r}{\epsilon_{max}} \tag{2}$$

where ϵ_r is the residual strain as defined above, and ϵ_{max} is the maximum experienced strain of the loading–unloading cycle.[55] As shown in Figure 2g, the AcAG/PAAm fc-DN hydrogels exhibit an extremely low residual strain ratio r_r from 0.02 to 0.06 as the maximum strain ϵ_{max} increases from 1 to 13. The residual strain ratio r_r of fc-DN gel did not show significant dependence on the strain rate (Figure S11a, Supporting Information), where the r_r remained at 0.05 under strain rates between 1 and 10 min^{-1} ($\epsilon_{max} = 10$). In addition, the residual strain ratio of the AG/PAAm f-DN hydrogel is 0.04 ($\epsilon_{max} = 10$), similar to fc-DN hydrogels (Figure S11b, Supporting Information). The PAAm SN hydrogel is highly resilient (Figure S12, Supporting Information) and shows negligible residual strain ratio (<0.001). Overall, the fc-DN hydrogels show a toughness that is 2 to 100 times higher than that of other tough hydrogel systems with a low residual strain ratio ($r_r < 0.1$ at $\epsilon_{max} > 1$) due to its combination of high fracture strain and strength (Figure 2h,i). Here the comparison is limited to hydrogel systems with fracture strain lower than 25, considering load-bearing applicability, which thus does not include ultra-stretchable systems.[68,69] Comparisons between the fc-DN hydrogel and other reported tough hydrogels in terms of residual strain ratio and toughness can be found in Figure S13 and Table S2, Supporting Information.

2.3. Study of Toughening Mechanism by Cyclic Tensile Tests and SAXS Measurement

To determine the toughening mechanisms in the fc-DN hydrogel, we have further performed the mechanical characterization of the fc-DN hydrogels under cyclic tensile tests and microstructural analysis using in situ synchrotron small angle X-ray scattering (SAXS). The results are summarized in **Figure 3**. At the maximum strain of 7, a significant hysteresis loop in the first tensile loading–unloading cycle can be observed in Figure 3a for DA 30%, C_{AcAG} of 3 wt%, and C_{AAm} of 50 wt%, indicating a significant irreversible structural change and dissipation of energy during the first deformation cycle. The deformed fc-DN hydrogel almost completely recovered when the stress was removed, showing only a residual strain of 0.4. The second loading curve showed clear softening as the modulus decreased from 0.88 MPa in the pristine sample to 0.23 MPa. This is similar to the conventional DN hydrogel, where the first loading process causes irreversible damage to the brittle network.[23,40] From the second tensile cycle onward, the hydrogel showed small hysteresis loops that remained constant without changes, that is, the hydrogel became more resilient after the first cycle.[1,56] The resilience ratio, defined as $1 - r_r$,[57] in the first loading-unloading cycle is 0.943, which approaches 1 (>0.991) from the second cycle on. As a comparison, the PAAm SN hydrogel shows consistently overlapping loading–unloading curves and thus negligible hysteresis during cyclic tensile tests as shown in Figure S12, Supporting Information, a typical rubber elastic property.

Figure 3b shows the successive cyclic loading–unloading of fc-DN gels at different maximum strains. A significant hysteresis loop emerged even at small strains such as 1, indicating that the agarose fibrillar network has been irreversibly damaged via the pull-out of agarose chains at low strains (Figure S14, Supporting Information).[58,59] Under progressive strain, the AcAG/PAAm fc-DN hydrogels demonstrate history-dependent mechanical properties similar to Mullins effects in conventional rubbers.[60,61] The stress–strain curve strongly depends on the maximum strain experienced previously. The loading curve always follows the previous unloading curve until the maximum strain in the previous cycle, after which the loading curve follows the tensile curve of the pristine sample. For each new cycle with a larger strain, a large hysteresis loop and subsequent softening of the hydrogel can be observed. Similarly, the compressive loading–unloading curves of AcAG/PAAm fc-DN hydrogel also showed a large hysteresis loop in the first loading cycle, leading to a softening phenomenon in the subsequent cycles (Figure S15a, Supporting Information). The Mullins effect can be observed in fc-DN hydrogels when subjected to progressive step-strain compression as well, as demonstrated in Figure S15b, Supporting Information.

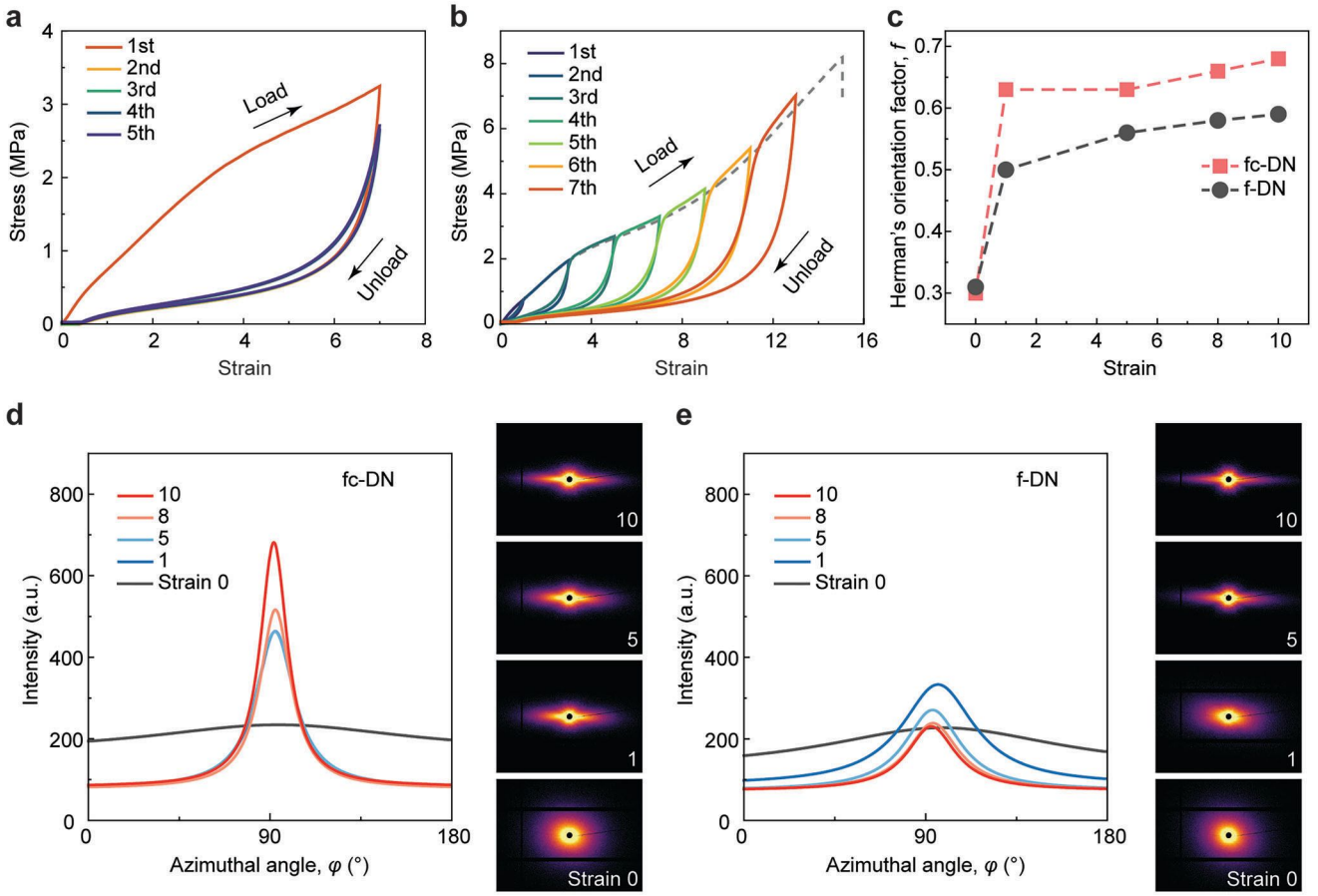

Figure 3. Cyclic loading–unloading tests of fc-DN hydrogels and in situ SAXS analysis. a,b) Cyclic tensile stress–strain curves of AcAG/PAAm fc-DN hydrogel. DA = 30%, C_{AcAG} = 3 wt%, C_{AAm} = 50 wt%. c) Calculated Herman's orientation factor f of fc-DN gels and f-DN gels at different strains. d,e) 2D SAXS plots and corresponding fitted azimuthal scan profiles of fc-DN gels (d) and f-DN gels (e). DA = 30%, $C_{AcAG} = C_{AG}$ = 3 wt%, C_{AAm} = 50 wt%, C_{CL} = 0.02 mol%.

For a more comprehensive understanding of the energy dissipation during the loading process of fc-DN gels, the amount of dissipated energy U_{hys} are shown as a function of maximum strains ϵ_{max} in Figure S16a, Supporting Information. The U_{hys} is defined by Equation (3) below.[58,62]

$$U_{hys} = \sum_{1}^{n} \Delta U_{hys\,i} \tag{3}$$

where U_{hys} is the total energy dissipated from the first cycle to the nth cycle, which is estimated by adding up the areas of the hysteresis loops $\Delta U_{hys\,i}$ in consecutive cycles. The U_{hys} of fc-DN gels and f-DN gels increased nonlinearly as a function of ϵ_{max}, similar to the previous report on DN hydrogel.[58] The U_{hys} of fc-DN gels was higher than that of f-DN gels, and this gap gradually increased as the maximum strain increased. To qualitatively assess the efficiency of energy dissipation, the relationship between U_{hys}/W and maximum strains was shown in Figure S16b, Supporting Information. Here W is the work done by extension to strain ϵ_n, which is estimated as follows[58,62]

$$W = U_{hys} + \int_{0}^{\epsilon_n} \sigma_{n+1} d\epsilon \tag{4}$$

where σ_{n+1} is the stress from the $(n+1)$th loading curve, and the ϵ_n is the maximum strain experienced strain up to nth cycle. The ratio U_{hys}/W represents the fraction of the irreversible work (dissipated energy) within W. After reaching the yielding point, U_{hys}/W of fc-DN gels and f-DN gels remained almost unchanged at ≈70% and 60%, respectively, regardless of the increase in strain. This result suggests that the energy dissipation efficiency of fc-DN gels is higher than that of f-DN gels, as 70% of the work was used for the irreversible damage of the agarose network in fc-DN gels, compared to 60% in f-DN gels. We thus propose that the higher energy dissipation efficiency in fc-DN gels compared to f-DN gels is a result of internetwork chemical crosslinks that result in stronger interfacial strength and better stress transfer between the two networks.

The AcAG/PAAm fc-DN hydrogel displays similar hysteresis and softening behaviors under cyclic loadings compared to reported DN hydrogels. Nevertheless, the AcAG/PAAm fc-DN hydrogel significantly outperforms the AG/PAAm f-DN hydrogel in their strength and toughness, suggesting differences in toughening mechanism between them. To further determine the microstructural changes inside hydrogels during deformations, in situ SAXS measurements of the hydrogels were performed at pre-defined strains. 2D SAXS plots, corresponding

azimuthal scan profiles, and calculated Herman's orientation factor (f) of fc-DN gels and f-DN gels at different strains are shown in Figure 3c–e. The azimuthal scan area and raw data can be found in Figure S17, Supporting Information. The calculation of f can be found in the Experimental Section. The scattering patterns of fc-DN gels became highly anisotropic with stronger intensity along the equatorial direction at a strain as low as 1, whereas the f-DN gels showed clear anisotropy at strains above 5. In contrast, PAAm SN hydrogels showed constant isotropic scattering patterns regardless of the strains (Figure S18, Supporting Information). Therefore, the anisotropic pattern indicates the alignment of agarose nanofibrillar bundles under stretching. This is also corroborated by the orders of magnitude weaker scattering intensity of PAAm SN hydrogel than that of agarose-containing hydrogels in the q range between 0.005 and 0.1 $Å^{-1}$ (Figure S19, Supporting Information), which corresponds to real-space distances from 6 to 126 nm, that is, the size range of heterogeneous fibril network of agarose (Figure S3, Supporting Information).

In the azimuthal scan profiles in Figure 3d,e (q range between ≈0.005 and 0.01 $Å^{-1}$), fc-DN gels featured sharp equatorial intensity maximum under deformations, indicating better alignment of the agarose fibrils in the fc-DN hydrogels compared to f-DN gels, which demonstrated relatively flat and broad peaks. This is also reflected in the orientation factor f of fc-DN gels, which increased to 0.63 at a strain of 1, compared to 0.50 in the case of f-DN hydrogel. The f continues to increase at higher strains, reaching 0.68 and 0.59 for fc-DN and f-DN at a strain of 10, respectively. The consistently higher f in the fc-DN than f-DN suggests that agarose fibrillar bundles inside fc-DN gels have a higher degree of alignment than those in the f-DN gels. This is the result of covalent bonds between the PAAm network and agarose network in fc-DN gels, which ensures efficient transfer of stress and deformation between the two networks. The higher degree of alignment and higher interfacial strength between the molecularly coiled PAAm network and agarose fibrillar network contribute to the enhanced strength and toughness in the fc-DN hydrogel. This strengthening mechanism is similar to fiber-reinforced composite materials, where higher interfacial strength and better alignment are beneficial for the mechanical properties of the composite materials.[63] Once the hydrogels returned to a strain of 0 after being stretched to a strain of 10, the scattering patterns of both fc-DN and f-DN became isotropic, which are similar to the pristine state (Figure S17,S18 Supporting Information), indicating non-permanent alignment of the agarose fibrils.

To further elucidate the importance of fibrillar agarose network and internetwork crosslinking for the toughening of the fc-DN hydrogel, we have implemented control experiments in the absence of AcAG fibrillar network or acrylate groups. Pretreating the AcAG gel with UV irradiation in the presence of a photoinitiator consumes the acrylate groups and reduces the internetwork crosslinks while inducing chemical crosslinks within the AcAG network. Such hydrogel showed a significant reduction in mechanical properties (Figure S5, Supporting Information), where the tensile strength and fracture strain approach that of the PAAm SN hydrogel. Besides, AcAG/PAAm hydrogel prepared at 55 °C showed a significant decrease in mechanical properties compared to the fc-DN gel (Figure S9, Supporting Information), as it lacks a fibrillar agarose network (see also SAXS data in Figure S19, Supporting Information). This is in accordance with the previous report on PAMPS/PAAm c-DN gel without a fibrillar network, where the chemical crosslinks between the two networks did not improve the mechanical properties compared to truly independent DN hydrogels.[47]

Based on the SAXS analysis and the mechanical properties of the fc-DN hydrogel, we propose the toughening mechanism of AcAG/PAAm fc-DN hydrogels illustrated in **Figure 4**. The agarose network is intrinsically brittle and stiff as shown in Figure S4, Supporting Information. Under small strains below 1, the agarose fibrils in both AG/PAAm f-DN and AcAG/PAAm fc-DN are aligned along the stretching direction as a result of a deformed PAAm network, where the fc-DN hydrogel undergoes a much higher degree of alignment compared to f-DN as shown by the in situ SAXS measurement. This indicates better stress transfer between the two networks via covalent bonds in the fc-DN hydrogels compared to f-DN. As the strain further increases to above 5, the agarose networks are damaged through pulling out of agarose chains,[58] which causes dissipation of energy and high toughness in the DN hydrogels. The fc-DN system shows a significant stiffening and strengthening effect in this strain range compared to f-DN hydrogel (Figure 1b), which can be attributed to the higher interfacial strength between the AcAG and PAAm network, resulting in a higher degree of chain pull-out. Upon further stretching to a strain above 12, the PAAm network in f-DN hydrogel fractures through the breaking of covalent bonds. In contrast, the internetwork covalent crosslinks in the fc-DN allow further pulling-out of agarose and a higher degree of fibril alignment, thus achieving higher fracture strain and strength. It is noted that there exist two processes during the stretching of the fc-DN hydrogels: 1) pull-out of agarose chains from the fibril bundles, which is an irreversible process, resulting in the high hysteresis and large energy dissipation during first loading-unloading; and 2) alignment of the agarose fibril bundles due to the deformation of the PAAm matrix, which is a reversible process, accounting for the observed anisotropy in the SAXS measurement. Since the residual strain is very small, the isotropy of the agarose fibril network fully recovers after the release of strain, as illustrated in Figure S20, Supporting Information. In summary, our results demonstrate that both the internetwork covalent bonds and the presence of a fibrillar network are essential for strengthening and toughening fc-DN gels, as a result of strong interface, efficient stress transfer and chain pull-out, and high alignment of agarose fibrils along the deformation direction.

2.4. Demonstrations of the fc-DN Hydrogels as Load-Bearing Components in Soft Devices

The superior toughness and strength of the fc-DN hydrogel are further demonstrated by their application in soft devices as load-bearing components, which can sustain, for example, deep puncture or high impact as shown in **Figure 5**. For the puncture test in Figure 5a, fc-DN and f-DN hydrogel films with a uniform thickness of 120 μm were synthesized and glued on the plastic rings with a diameter of 25 mm. The films were then subjected to puncture with a plastic flat-cap rod (diameter 5 mm) under varying weights. The experimental details of the puncture tests can be found in the Experimental Section and Figure S21, Supporting Information. As depicted in Figure 5a, when subjected to 300 g

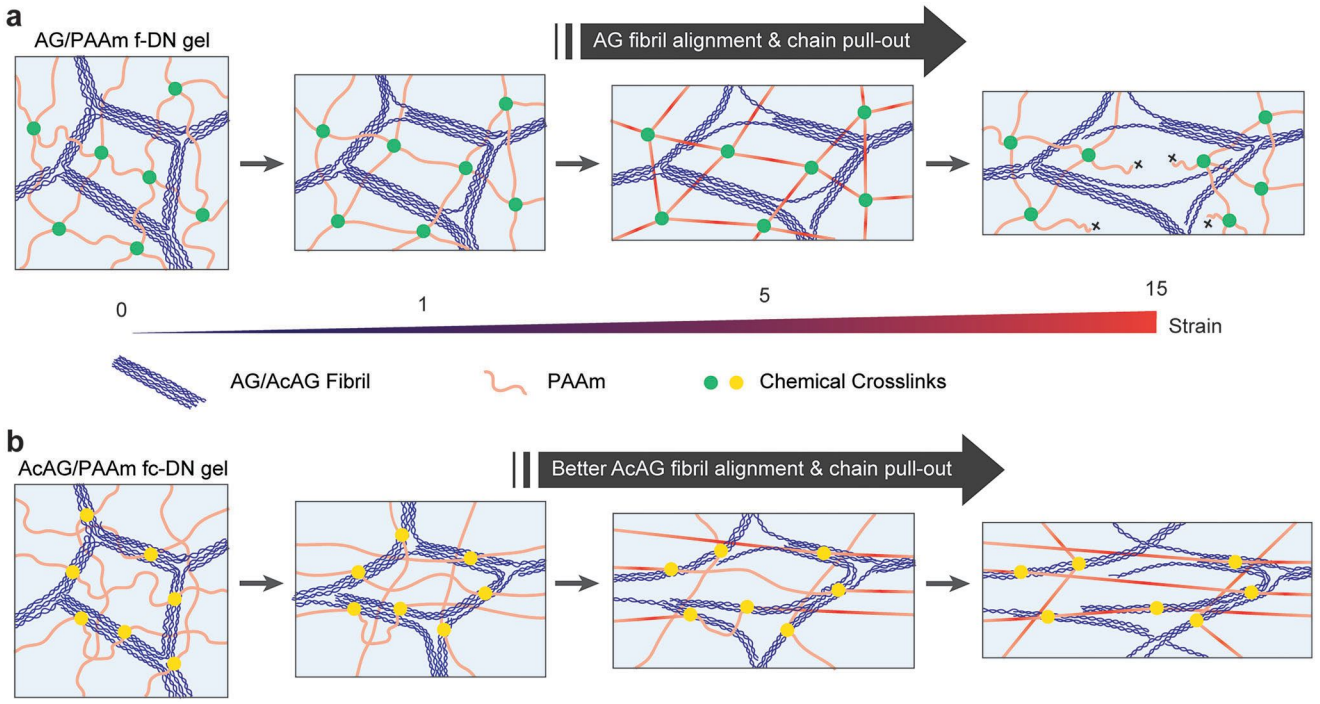

Figure 4. Schematic illustrations of toughening mechanism in the fc-DN hydrogel. Illustrations of f-DN hydrogel (a) and fc-DN hydrogel (b) under increasing strains. The numbers of PAAm chains are reduced for clarity.

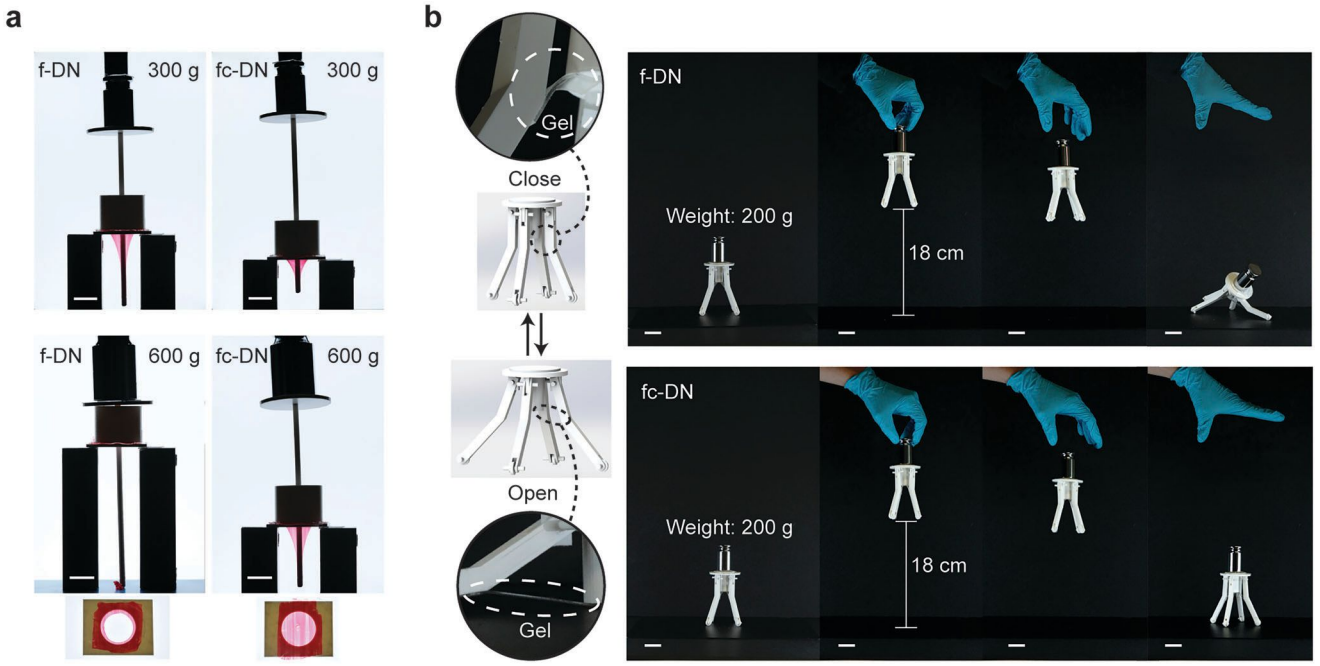

Figure 5. Demonstrations of fc-DN hydrogel as load-bearing components with improved performances compared to f-DN hydrogels. a) Comparisons of the AG/PAAm f-DN hydrogel and the AcAG/PAAm fc-DN hydrogel when subjected to puncture. Scale bars: 2 cm. Hydrogels were dyed for better visibility. b) Comparisons of the AG/PAAm f-DN hydrogel and the AcAG/PAAm fc-DN hydrogel as load-bearing components for free-falling landers. Weight: 200 g. Scale bars: 5 cm.

weights, the f-DN hydrogel experiences notable deformation of 3.1 cm (measured by the distance from the tip of the rod to the initial position of the film), which is 2.2 times greater than that observed in the fc-DN hydrogel (1.4 cm). With an increased weight of 600 g, the f-DN hydrogel succumbed to puncture-through failure, while the fc-DN hydrogel retained its structural integrity and remained undamaged once the load was removed (Figure 5a, photo inset).

The toughness and impact-resistant performance of the fc-DN hydrogel is further demonstrated by a soft lander undergoing falling-induced impact, where the hydrogels serve as load-bearing belts of the landing legs, as shown in Figure 5b. The lander was fabricated by 3D printing of plastic as detailed in the Experimental Section and had four jointed legs that could open and close freely, as shown in Figure 5b. Four pieces of hydrogel belts (6 mm × 20 mm × 1 mm) were attached by super glue to link the legs with the central body so that they serve as the load-bearing parts of the lander when it is subjected to static or impact load in the vertical direction. The lander was elevated to a height of 18 cm with a weight of 200 g attached (total weight ≈224 g) and then released to undergo freefalling. The impact of landing was absorbed by the transient elongation of the hydrogel belts, which is akin to the function of tendons. As a result, the lander assembled with f-DN hydrogels could not withstand the impact during landing, as the f-DN hydrogel failed to return to the original position at the first trial (Figure 5b), and eventually broke at the second trial (Figure S22a and Video S1, Supporting Information). In contrast, fc-DN hydrogels could sustain the impact and stabilize the landing upon freefalling, even after ten attempts (Figure S22b and Video S1, Supporting Information). The demonstrations above show the improved mechanical properties of the fc-DN hydrogels compared to the conventional f-DN design and their application potential in soft devices as load-bearing components.

3. Conclusion

We report a new toughening strategy to prepare strong and tough hydrogels based on fc-DN. The fc-DN consists of a molecularly coiled PAAm network chemically crosslinked by an AcAG fibrillar network, forming an interconnected interpenetrating network. The resulting AcAG/PAAm fc-DN hydrogel exhibits dramatically increased strength (8 MPa) and toughness (55 MJ m^{-3}) compared to the AG/PAAm f-DN hydrogel. Due to the chemical crosslinking between the nanofibrillar and molecular networks, the hydrogel also exhibits low residual strain (0.5) after experiencing a high tensile strain of 10, a notable property compared to reported tough hydrogels. Compared to conventional f-DN hydrogels without internetwork chemical crosslinks, the covalent bonds between the networks of fc-DN hydrogels result in stronger interfacial strength between the two networks and a higher degree of agarose fibril alignment under strain as corroborated by in situ SAXS measurement. Compared to c-DN hydrogels, the fibrillar agarose network allows higher energy dissipation due to the pull-out of agarose chains and higher strength due to the alignment of fibrils. The superior mechanical properties are demonstrated by soft devices where the fc-DN hydrogels serve as the load-bearing components under puncture or impact. The fc-DN design strategy provides a new avenue to fabricate hydrogels with high mechanical strength, toughness, and low plastic deformations, which promises great potential for applications in soft robotics, artificial skins, and bioelectronics.

4. Experimental Section

Materials: Acryloyl chloride, agarose (A9539), acrylamide, *N,N′*-methylenebis(acrylamide) (BIS), acetone, *N,N*-dimethylacetamide (DMAc), and the photoinitiator Irgacure 2959 were purchased from Sigma and used as received without further purification. Deionized water (18.2 MΩ; DirectQ 3 UV; Millipore) was used throughout the experiments.

Modification of Agarose: Agarose (0.4 g) was dissolved in DMAc (15 mL) at 90 °C. The solution was then cooled in an ice-water bath and a suitable amount (10, 20, 30, 60, 100, and 200 µL) of acryloyl chloride diluted in DMAc (1 mL) was added slowly under stirring. The mixture was continuously stirred at 0 °C for 1 h and then at room temperature for 4 h. The product was precipitated and washed thoroughly by acetone and then dried in a vacuum.

Calculation of Degree of Substitution: The degree of substitution was determined by ^{1}H-NMR, with dimethyl sulfoxide-*d6* used as the solvent. The appearance of signals from protons of acryloyl groups (—CO—CH=CH_2) in the ^{1}H NMR spectrum between 5.9 and 6.4 ppm proved the partial acrylation of agarose.[48] The degree of substitution was calculated from the integral ratio of the signals at 5.9–6.4 ppm and that of the signals at around 5.1 ppm from protons at position 1 in 3,6 anhydro-α-L-galactopyranose unit of agarose, which were used as internal standard.[64]

Preparation of AcAG/PAAm fc-DN Hydrogels: Briefly, AcAG (30 mg), AAm (500 mg), photoinitiator (1 mg), and DI water (470 µL) were added into a vial. The vial was vortexed and heated to 90 °C using a heat gun until AcAG was fully dissolved, resulting in a transparent solution. The resulting solution was degassed and then injected into a rectangular glass mold with Parafilm serving as a spacer. The mold was cooled at 4 °C in a refrigerator to facilitate the gelation of AcAG, which was then photopolymerized with UV light (365 nm wavelength, 6 W) for 2 h to form an AcAG/PAAm fc-DN hydrogel. To prepare the AG/PAAm f-DN hydrogel, a similar method was used, but AcAG was replaced with AG.

Mechanical Measurements: Samples of hydrogels were cut into dumbbell shapes with a gauge width of 2 mm using a metallic cutter. The thickness of the individual samples was measured using a caliper, typically around 1 mm. Tension and compression tests were conducted on a tensile machine (Instron 5567; 100 N load cell) with a stretching deformation rate of 5 min^{-1} and a compressing deformation rate of 0.5 min^{-1}. Cylindrical samples were used in compression tests. Each test was repeated for at least three times.

Fracture Toughness: The fracture toughness was measured through a unilateral crack test with a stretching rate of 5 min^{-1}, following the method in reference.[65] The samples were cut into rectangular shapes with a size of 20 mm × 4 mm × 1 mm. The initial crack length was 1 mm. Fracture toughness *G* was calculated using the following equation

$$G = \frac{6Wl}{\sqrt{\lambda}} \tag{5}$$

where λ is the fracture strain when the edge-notched samples were subjected to uniaxial stretching, *W* is the strain energy density of an uncracked sample being stretched to the maximum strain λ, and *l* is the initial crack length.

In Situ Small-Angle X-ray Scattering: In situ SAXS measurements of hydrogels under different strains were conducted at the beamline I22 of Diamond Light Source, United Kingdom. The X-ray wavelength was 0.62 Å (20 kV) and the sample-to-detector distances were 9.7 m. Dumbbell-shaped specimens were stretched to pre-defined strains by a homemade tensile machine, after which the SAXS data were collected with an exposure time of 10 s. The beam diameter was around 20 µm and the sample thickness before stretch was 2 mm. The 2D patterns were obtained using a Pilatus P3-2M detector (DECTRIS, Switzerland). The corresponding 1D

profiles were extracted by integration using DAWN software with air used for background subtraction.[66] For all azimuthal scan profiles, the q range was between ≈0.005 and 0.01 Å^{-1}.

Puncture Test: A hydrogel film with a thickness of ≈120 µm was glued to a rigid plastic ring with an inner diameter of 25 mm. The hydrogel film was dyed using a marker pen for better visibility. A plastic rod with a diameter of 5 mm was then placed above the middle of the hydrogel. This arrangement was then gently weighted down, allowing for a gradual puncture on the hydrogel.

Design and Fabrication of Lander: The lander incorporated four legs mounted to the bottom of a load platform via axles. Each leg was equipped with a wheel at its end to minimize friction during landing. All these plastic parts of the lander were custom-designed in SolidWorks and fabricated with PLA filaments using a 3D-printing system (Ultimaker S3). The hydrogel was cut into belts measuring 6 mm × 20 mm × 1 mm. Subsequently, these belts were affixed between the legs and the central pillar of the lander, as depicted in the close-up view presented in Figure 5b. After loading a 200 g weight on the top of the platform, the lander was released from a height of 18 cm.

Video and Photo Capture: All movies and photos were captured by a Canon 5D Mark IV camera equipped with a Canon Zoom Lens EF 24–70 mm f/2.8L II USM.

Statistical Analysis: All tests were repeated three times and data were represented as the mean ± standard deviation (SD). All statistical analyses were conducted using Origin software.

Supporting Information

Supporting Information is available from the Wiley Online Library or from the author.

Acknowledgements

The authors thank Prof. Heikki Tenhu for the discussions on Mullins effect, Xiaodan Hong for SEM measurement, and the provision of facilities and technical support by Aalto University at OtaNano – Nanomicroscopy Center (Aalto-NMC). The authors are grateful to Diamond Light Source for providing synchrotron beam time (SM34102-1) at beamline I22 and specifically acknowledge the support from Dr. Olga Shebanova, Dr. Tim Snow, and Prof. Himadri Gupta during our in situ SAXS experiments. The authors acknowledge funding from the Academy of Finland (Postdoctoral Researcher No. 331015 to H.Z., Postdoctoral Researcher No. 330214 to Z.-P.L. and Center of Excellence in Life-Inspired Hybrid Materials – LIBER No. 346108 to O.I.), China Scholarship Council (No. 202207960015 to Y.-H.F.) and the European Research Council (Advanced Grant DRIVEN No. 742829 to O.I.).

Conflict of Interest

The authors declare no conflict of interest.

Data Availability Statement

The data that support the findings of this study are available from the corresponding author upon reasonable request.

Keywords

double networks, hydrogels, interpenetrating polymer networks, polysaccharides, toughness

Received: February 13, 2024
Revised: March 19, 2024
Published online: April 5, 2024

[1] X. Zhao, X. Chen, H. Yuk, S. Lin, X. Liu, G. Parada, *Chem. Rev.* **2021**, *121*, 4309.
[2] G. A. Johnson, D. M. Tramaglini, R. E. Levine, K. Ohno, N.-Y. Choi, S. L.-Y. Woo, *J. Orthop. Res.* **1994**, *12*, 796.
[3] I. Vesely, *J. Biomech.* **1997**, *31*, 115.
[4] B. K. Connizzo, S. M. Yannascoli, L. J. Soslowsky, *Matrix Biol.* **2013**, *32*, 106.
[5] L. Han, E. H. Frank, J. J. Greene, H.-Y. Lee, H.-H. K. Hung, A. J. Grodzinsky, C. Ortiz, *Biophys. J.* **2011**, *100*, 1846.
[6] H. Furukawa, K. Horie, R. Nozaki, M. Okada, *Phys. Rev. E* **2003**, *68*, 31406.
[7] J. Bastide, L. Leibler, *Macromolecules* **1988**, *21*, 2647.
[8] H. J. Zhang, T. L. Sun, A. K. Zhang, Y. Ikura, T. Nakajima, T. Nonoyama, T. Kurokawa, O. Ito, H. Ishitobi, J. P. Gong, *Adv. Mater.* **2016**, *28*, 4884.
[9] M. A. Gonzalez, J. R. Simon, A. Ghoorchian, Z. Scholl, S. Lin, M. Rubinstein, P. Marszalek, A. Chilkoti, G. P. López, X. Zhao, *Adv. Mater.* **2017**, *29*, 1604743.
[10] T. L. Sun, T. Kurokawa, S. Kuroda, A. B. Ihsan, T. Akasaki, K. Sato, M. A. Haque, T. Nakajima, J. P. Gong, *Nat. Mater.* **2013**, *12*, 932.
[11] T. Long, Y. Li, X. Fang, J. Sun, *Adv. Funct. Mater.* **2018**, *28*, 1804416.
[12] X. Li, K. Cui, T. L. Sun, L. Meng, C. Yu, L. Li, C. Creton, T. Kurokawa, J. P. Gong, *Proc. Natl. Acad. Sci. USA* **2020**, *117*, 7606.
[13] X. Hu, M. Vatankhah-Varnoosfaderani, J. Zhou, Q. Li, S. S. Sheiko, *Adv. Mater.* **2015**, *27*, 6899.
[14] Y. J. Wang, X. N. Zhang, Y. Song, Y. Zhao, L. Chen, F. Su, L. Li, Z. L. Wu, Q. Zheng, *Chem. Mater.* **2019**, *31*, 1430.
[15] Y. Zhang, Y. Li, W. Liu, *Adv. Funct. Mater.* **2015**, *25*, 471.
[16] J.-Y. Sun, X. Zhao, W. R. K. Illeperuma, O. Chaudhuri, K. H. Oh, D. J. Mooney, J. J. Vlassak, Z. Suo, *Nature* **2012**, *489*, 133.
[17] P. Lin, S. Ma, X. Wang, F. Zhou, *Adv. Mater.* **2015**, *27*, 2054.
[18] H. C. Yu, S. Y. Zheng, L. Fang, Z. Ying, M. Du, J. Wang, K.-F. Ren, Z. L. Wu, Q. Zheng, *Adv. Mater.* **2020**, *32*, 2005171.
[19] A. Harada, Y. Takashima, M. Nakahata, *Acc. Chem. Res.* **2014**, *47*, 2128.
[20] W. Wang, R. Narain, H. Zeng, *Front. Chem.* **2018**, *6*, 497.
[21] E. Prince, E. Kumacheva, *Nat. Rev. Mater.* **2019**, *4*, 99.
[22] Q. He, Y. Huang, S. Wang, *Adv. Funct. Mater.* **2018**, *28*, 1705069.
[23] Q. Chen, L. Zhu, C. Zhao, Q. Wang, J. Zheng, *Adv. Mater.* **2013**, *25*, 4171.
[24] Z. Wang, X. Zheng, T. Ouchi, T. B. Kouznetsova, H. K. Beech, S. Av-Ron, T. Matsuda, B. H. Bowser, S. Wang, J. A. Johnson, J. A. Kalow, B. D. Olsen, J. P. Gong, M. Rubinstein, S. L. Craig, *Science* **2021**, *374*, 193.
[25] B. Bao, Q. Zeng, K. Li, J. Wen, Y. Zhang, Y. Zheng, R. Zhou, C. Shi, T. Chen, C. Xiao, B. Chen, T. Wang, K. Yu, Y. Sun, Q. Lin, Y. He, S. Tu, L. Zhu, *Nat. Mater.* **2023**, *22*, 1253.
[26] Y. Yang, X. Wang, F. Yang, H. Shen, D. Wu, *Adv. Mater.* **2016**, *28*, 7178.
[27] M. Hua, S. Wu, Y. Ma, Y. Zhao, Z. Chen, I. Frenkel, J. Strzalka, H. Zhou, X. Zhu, X. He, *Nature* **2021**, *590*, 594.
[28] J. P. Gong, Y. Katsuyama, T. Kurokawa, Y. Osada, *Adv. Mater.* **2003**, *15*, 1155.
[29] M. T. I. Mredha, Y. Z. Guo, T. Nonoyama, T. Nakajima, T. Kurokawa, J. P. Gong, *Adv. Mater.* **2018**, *30*, 1704937.
[30] S. Lin, J. Liu, X. Liu, X. Zhao, *Proc. Natl. Acad. Sci. U. S. A.* **2019**, *116*, 10244.
[31] X. Liang, G. Chen, S. Lin, J. Zhang, L. Wang, P. Zhang, Y. Lan, J. Liu, *Adv. Mater.* **2022**, *34*, 2107106.
[32] X. Liang, G. Chen, I. M. Lei, P. Zhang, Z. Wang, X. Chen, M. Lu, J. Zhang, Z. Wang, T. Sun, Y. Lan, J. Liu, *Adv. Mater.* **2023**, *35*, 2207587.
[33] J. Kim, G. Zhang, M. Shi, Z. Suo, *Science* **2021**, *374*, 212.
[34] G. Nian, J. Kim, X. Bao, Z. Suo, *Adv. Mater.* **2022**, *34*, 2206577.
[35] L. Fu, L. Li, Q. Bian, B. Xue, J. Jin, J. Li, Y. Cao, Q. Jiang, H. Li, *Nature* **2023**, *618*, 740.

[36] P. Matricardi, C. Di Meo, T. Coviello, W. E. Hennink, F. Alhaique, *Adv. Drug Delivery Rev.* **2013**, *65*, 1172.
[37] M. S. Silverstein, *Polymer* **2020**, *207*, 122929.
[38] J. Yang, Y. Li, L. Zhu, G. Qin, Q. Chen, *J. Polym. Sci., Part B: Polym. Phys.* **2018**, *56*, 1351.
[39] G. He, H. Lei, W. Sun, J. Gu, W. Yu, D. Zhang, H. Chen, Y. Li, M. Qin, B. Xue, W. Wang, Y. Cao, *Angew. Chem., Int. Ed.* **2022**, *61*, 202201765.
[40] J. P. Gong, *Soft Matter* **2010**, *6*, 2583.
[41] T. Yasui, Y. Zheng, T. Nakajima, E. Kamio, H. Matsuyama, J. P. Gong, *Macromolecules* **2022**, *55*, 9547.
[42] F. Yang, V. Tadepalli, B. J. Wiley, *ACS Biomater. Sci. Eng.* **2017**, *3*, 863.
[43] T. Matsuda, R. Kawakami, R. Namba, T. Nakajima, J. P. Gong, *Science* **2019**, *363*, 504.
[44] L. Wang, G. Shan, P. Pan, *Soft Matter* **2014**, *10*, 3850.
[45] F. Ding, W. Tang, L. Fu, R. Zhang, G. Wang, Z. Han, R. Wu, Y. Dong, X. Zou, *Polymer* **2022**, *238*, 124387.
[46] S. Hu, Y. Fang, C. Liang, M. Turunen, O. Ikkala, H. Zhang, *Nat. Commun.* **2023**, *14*, 3717.
[47] T. Nakajima, H. Furukawa, Y. Tanaka, T. Kurokawa, Y. Osada, J. P. Gong, *Macromolecules* **2009**, *42*, 2184.
[48] A. Pourjavadi, S. S. Afjeh, F. Seidi, H. Salimi, *J. Appl. Polym. Sci.* **2011**, *122*, 2424.
[49] K. Bertula, L. Martikainen, P. Munne, S. Hietala, J. Klefström, O. Ikkala, Nonappa, *ACS Macro Lett.* **2019**, *8*, 670.
[50] Y. Kawauchi, Y. Tanaka, H. Furukawa, T. Kurokawa, T. Nakajima, Y. Osada, J. P. Gong, *J. Phys.: Conf. Ser.* **2009**, *184*, 012016.
[51] Y. Wang, G. Nian, J. Kim, Z. Suo, *J. Mech. Phys. Solids* **2023**, *170*, 105099.
[52] R. J. Wagner, J. Dai, X. Su, F. J. Vernerey, *J. Mech. Phys. Solids* **2022**, *167*, 104982.
[53] P. J. Flory, N. Rabjohn, M. C. Shaffer, *J. Appl. Polym. Sci.* **1949**, *4*, 435.
[54] K. Kothari, Y. Hu, S. Gupta, A. Elbanna, *J. Appl. Mech.* **2018**, *85*, 031008.
[55] J. Liu, M. Li, X. Li, W. Yan, W. Huang, S. Yan, *J. Alloys Compd.* **2019**, *781*, 621.
[56] S. Lin, Y. Zhou, X. Zhao, *Extreme Mech. Lett.* **2014**, *1*, 70.
[57] W. Feng, J. Li, Y. Feng, M. Qin, *RSC Adv.* **2014**, *4*, 10090.
[58] Q. Chen, L. Zhu, L. Huang, H. Chen, K. Xu, Y. Tan, P. Wang, J. Zheng, *Macromolecules* **2014**, *47*, 2140.
[59] M. Zhang, D. Zhang, H. Chen, Y. Zhang, Y. Liu, B. Ren, J. Zheng, *npj Comput. Mater.* **2021**, *7*, 39.
[60] L. Mullins, *Rubber Chem. Technol.* **1969**, *42*, 339.
[61] R. E. Webber, C. Creton, H. R. Brown, J. P. Gong, *Macromolecules* **2007**, *40*, 2919.
[62] T. Nakajima, T. Kurokawa, S. Ahmed, W. Wu, J. P. Gong, *Soft Matter* **2013**, *9*, 1955.
[63] K. L. Pickering, M. G. A. Efendy, T. M. Le, *Composites, Part A* **2016**, *83*, 98.
[64] A. Gamini, R. Toffanin, E. Murano, R. Rizzo, *Carbohydr. Res.* **1997**, *304*, 293.
[65] R. Long, C.-Y. Hui, *Soft Matter* **2016**, *12*, 8069.
[66] J. Filik, A. W. Ashton, P. C. Y. Chang, P. A. Chater, S. J. Day, M. Drakopoulos, M. W. Gerring, M. L. Hart, O. V. Magdysyuk, S. Michalik, A. Smith, C. C. Tang, N. J. Terrill, M. T. Wharmby, H. Wilhelm, *J. Appl. Crystallogr.* **2017**, *50*, 959.
[67] S. Tan, C. Wang, B. Yang, J. Luo, Y. Wu, *Adv. Mater.* **2022**, *34*, https://doi.org/10.1002/adma.202206904.
[68] W. Li, X. Wang, Z. Liu, X. Zou, Z. Shen, D. Liu, L. Li, Y. Guo, F. Yan, *Nature Materials* **2023**, *23*, 131.